SPECIAL TOPIC

High-pressure synthesis of an oxynitride perovskite $CeNbO_2N$ with Nb^{4+} charge state

To cite this article: Shengjie Liu *et al* 2025 *Chinese Phys. B* **34** 066202

SPECIAL TOPIC — Structures and properties of materials under high pressure

High-pressure synthesis of an oxynitride perovskite $CeNbO_2N$ with Nb^{4+} charge state

Shengjie Liu(刘胜杰)[1,2], Xubin Ye(叶旭斌)[2], Zhao Pan(潘昭)[2,3], Jie Zhang(张杰)[2,3], Shuai Tang(唐帅)[2,3], Guangkai Zhang(张广凯)[2,4], Maocai Pi(皮茂材)[2,3], Zhiwei Hu(胡志伟)[5], Chien-Te Chen(陈建德)[6], Ting-Shan Chan(詹丁山)[6], Cheng Dong(董成)[2], Tian Cui(崔田)[1], Yanping Huang(黄艳萍)[1], Zhenhua Chi(迟振华)[7,†], Yao Shen(沈瑶)[2,3,‡], and Youwen Long(龙有文)[2,3,8,§]

[1] *Institute of High Pressure Physics, School of Physical Science and Technology, Ningbo University, Ningbo* 315211, *China*
[2] *Beijing National Laboratory for Condensed Matter Physics, Institute of Physics, Chinese Academy of Sciences, Beijing* 100190, *China*
[3] *School of Physical Sciences, University of Chinese Academy of Sciences, Beijing* 100049, *China*
[4] *Department of Physics, Shanghai Normal University, Shanghai* 200234, *China*
[5] *Max Planck Institute for Chemical Physics of Solids, Nöthnitzer Straße* 40, 01187 *Dresden, Germany*
[6] *National Synchrotron Radiation Research Center (NSRRC), Hsinchu Science Park, Hsinchu* 300092, *Taiwan, China*
[7] *Institute of Plasma Physics, HFIPS, Chinese Academy of Sciences, Hefei* 230031, *China*
[8] *Songshan Lake Materials Laboratory, Dongguan* 523808, *China*

(Received 12 March 2025; revised manuscript received 27 March 2025; accepted manuscript online 28 March 2025)

Perovskite oxynitrides $AB(N,O)_3$, a crucial class in materials science, have attracted much attention. By precisely controlling *A*- and *B*-site ions and tuning the N/O ratio, new materials with exotic charge states and intriguing electronic behaviors can be designed and synthesized. In this work, a novel oxynitride perovskite, $CeNbO_2N$, was prepared under high-temperature and high-pressure conditions. The compound crystallizes in an orthorhombic perovskite structure in *Pnma* symmetry with disordered N/O distribution. The x-ray absorption spectroscopy confirms the presence of a Nb^{4+} state with $4d^1$ electronic configuration in $CeNbO_2N$. As a result, the resistivity of $CeNbO_2N$ is sharply reduced compared to its counterpart $CeTa^{5+}ON_2$ and other Nb^{5+} compounds. No long-range spin order is found to occur with the temperature down to 2 K in $CeNbO_2N$, while a remarkable negative magnetoresistance effect shows up at lower temperatures, probably due to the magnetic scattering arising from short-range spin correlations.

Keywords: high-pressure synthesis, oxynitride perovskite, spin correlation

PACS: 62.50.–p, 72.80.Ga, 75.47.–m

DOI: 10.1088/1674-1056/adc668 **CSTR:** 32038.14.CPB.adc668

1. Introduction

Perovskite-type materials, with the general chemical formula ABX_3, have received much attention in condensed matter physics and materials science, owing to the wide variety of intriguing physical properties and promising applications in numerous fields such as catalysis,[1] energy storage,[2] information storage,[3,4] magnetism,[5–8] and optics.[9–11] Among the various sub-classes of perovskite-type materials, $AB(N,O)_3$-type perovskite oxynitrides have emerged as a particularly intriguing and rapidly evolving category of functional materials in recent years.[12–15] In these compounds, nitrogen partially or fully substitutes for oxygen in the traditional perovskite structure. This substitution alters the coordination environment and chemical bonding of transition-metal ions, which has a profound impact on both the electronic structure and magnetic properties of the materials.[7,8] The physical properties can be further tuned by the exact control of the elements and valence states of *A*- and *B*-site cations. For example, in the family of $LnMO_{3-x}N_x$ (Ln = rare-earth or alkaline earth metal, M = transition metal), $BaTaO_2N$ presents a high dielectric constant,[16] while $EuNbO_2N$ is ferromagnetic and shows colossal magnetoresistance effects.[17] $MnTaO_2N$, on the other hand, exhibits a helical spin order, which is in sharp contrast with the isostructural $MnTiO_3$ that shows G-type antiferromagnetism.[14] $RTiNO_2$ (R = Ce, Pr, Nd) compounds are paramagnetic, with the Curie–Weiss temperature ranging from 28 K to 42 K,[18] while $CeTaN_2O$ is an antiferromagnetic semiconductor, with a magnetic phase transition temperature below 2 K.[19] Additionally, $LaReN_3$ exhibits metallic conductivity with Pauli paramagnetism,[20] and $LaWN_3$ demonstrates a large piezoelectric response.[21]

Although perovskite oxynitrides provide a new strategy for the rational design and development of novel magnetic materials with tailored functional properties, challenges per-

†Corresponding author. E-mail: zhchi@issp.ac.cn
‡Corresponding author. E-mail: yshen@iphy.ac.cn
§Corresponding author. E-mail: ywlong@iphy.ac.cn

sist regarding the precise control over their crystal structure, stoichiometric composition, and defect concentration during synthesis. Furthermore, the complex relationship between their structural characteristics and functional properties remains elusive, hindering the advancement and practical application of these materials.[17,22–24] In this work, we successfully synthesized a novel perovskite oxynitride, $CeNbO_2N$. Through detailed structural refinement, it was found that the N and O atoms are disorderly distributed in the $CeNbO_2N$ lattice, which crystallizes in the *Pnma* space group. Different from most Nb-based compounds, a relatively rare Nb^{4+} charge state with a $4d^1$ electronic configuration is found to occur in $CeNbO_2N$, suggesting the presence of itinerant electronic behavior with the absence of long-range spin order.

2. Experimental details

The oxide precursor $CeNbO_4$ was first prepared with CeO_2 (with a purity of 99.99%) and Nb_2O_5 (with a purity of 99.99%) as the starting materials. These two reactants were thoroughly mixed in a molar ratio of 2:1 and transferred into a muffle furnace, calcined at 1350 °C for 10 h, and followed by an additional calcination at 800 °C for 10 h.[25] During the calcination process, the Ar gas was introduced to prevent the formation of impurities. High-purity $CeNbO_4$ can be obtained after furnace cooling. $NaNH_2$ with a purity of 99.0% was used as the nitrogen-supplying reagent. It was mixed with $CeNbO_4$ in a molar ratio of 8:1 and thoroughly ground. The resulting mixture was charged into a tantalum capsule with 6 mm in both diameter and height. Since $NaNH_2$ is air-sensitive, the grinding and assembling processes were conducted within an argon-filled glove box. A cubic-anvil-type high-pressure apparatus was utilized to generate high-temperature and high-pressure conditions of 3 GPa and 1770 K for a duration of 1 h. Afterwards, the sample underwent quenching before the pressure was gradually released. The obtained bulk sample was pulverized into powder and rinsed with deionized water to eliminate the impurity by-products such as NaOH.[19] High purity polycrystalline $CeNbO_2N$ sample was acquired after subsequent desiccation.

Powder synchrotron x-ray diffraction (SXRD) was measured at the BL02B2 ($\lambda = 0.65$ Å) beamline of SPring-8, Japan. The 2θ scan ranged from 5° to 55° with a step size of 0.006°. The Rietveld refinement was carried out using the GSAS software.[26] The x-ray absorption spectra (XAS) at the Ce-$M_{4,5}$ and Nb-L_3 edges were measured at room temperature at the TLS11A and TLS16A beamlines of the National Synchrotron Radiation Research Center using the total electron yield mode and fluorescence yield mode, respectively. Magnetic susceptibility and isothermal magnetization were measured using a Quantum Design superconducting quantum interference device magnetometer (MPMS-SQUID). For magnetic susceptibility measurements, both zero-field-cooling (ZFC) and field-cooling (FC) modes were applied under a magnetic field of 0.1 T. Specific heat and electrical transport properties were measured using a quantum design physical property measurement system (PPMS-9T).

3. Results and discussion

Figure 1 shows the SXRD pattern and Rietveld refinement results of $CeNbO_2N$ collected at room temperature, indicating the high quality of the sample. All the diffraction peaks can be described by the orthorhombic space group *Pnma* with the lattice constants of $a = 5.70204(3)$ Å, $b = 8.05436(3)$ Å, and $c = 5.71185(2)$ Å. The reasonable goodness-of-fit factors, $R_{wp} = 2.67\%$ and $R_p = 1.58\%$, suggest the reliability of the refinement results. According to the refinement, the anions are found to be randomly distributed, with each anionic site occupied by 2/3 of O and 1/3 of N. The detailed refined parameters, bond lengths, and bond angles of $CeNbO_2N$ are listed in Table 1.

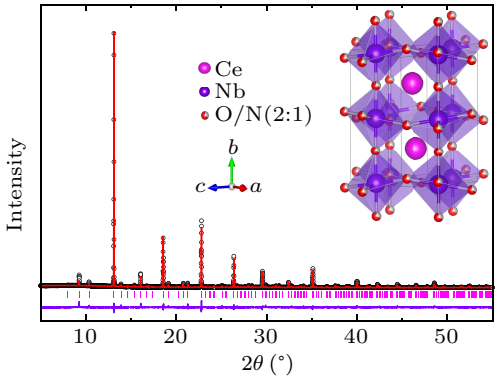

Fig. 1. SXRD pattern and Rietveld refinement of $CeNbO_2N$. The black circles, red lines and violet lines indicate the observed, calculated and difference, respectively. The ticks indicate the allowed Bragg reflections for space group *Pnma*. The inset displays the crystal structure of $CeNbO_2N$, where Ce, Nb, O, and N are shown in magenta, purple, red, and gray-violet, respectively.

It is well known that XAS is an element-selective tool to explore the valence states. The multiplet interaction is dominant in the XAS spectra at the rare-earth $M_{4,5}$ edges, namely, each $4f^n$ configuration in the ground state has its characteristic $3d^9 4f^{n+1}$ multiplet spectral feature in the XAS final states. For Ce^{4+} compounds, the higher energy satellite at 890 eV is a fingerprint for $4f^0$ configuration as depicted in Fig. 2(a).[27] The Ce $M_{4,5}$-spectrum of $CeNbO_2N$ is the same as that of Ce_2O_3, indicating a Ce^{3+} valence state in $CeNbO_2N$. There is no detectable spectral feature at 890 eV, indicating pure Ce^{3+} state.[28,29] Figure 2(b) shows the Nb L_3-edge XAS spectrum of $CeNbO_2N$, along with those of $NbMoO_4$ and Nb_2O_5 as Nb^{4+} and Nb^{5+} references, respectively. The XAS spectral feature at the $L_{2,3}$ edges of 4d transition oxide is mainly determined by crystal field interaction, the energy position of the white line shifts to higher energy by about 1 eV or more with an increase of valence state by one.[30,31]

Table 1. Refinement structural parameters for $CeNbO_2N$ based on the SXRD data collected at room temperature. The sum of the occupancies of N and O atoms at the same Wyckoff position was fixed to be 1.

Space group					*Pnma*
Atomic position(s)					
Atom	*x*	*y*	*z*	Occupancy	$U_{iso} \times 100$ Å^2
Ce (4*c*)	0.01994(1)	0.25004(3)	1.0080(3)	1	1.1(2)
Nb (4*b*)	0.5	0	0	1	3.3(3)
N1 (4*c*)	0.49647(3)	0.2500	0.00271(7)	0.33	3.6(4)
O1 (4*c*)	0.49647(3)	0.2500	0.00271(7)	0.67	3.6(4)
N2 (8*d*)	0.30320(2)	0.04274(1)	0.70112(2)	0.33	1.7(3)
O2 (8*d*)	0.30320(2)	0.04274(1)	0.70112(2)	0.67	1.7(3)
Bond lengths					
Ce–N1/O1 (Å)	2.718(15), 2.80(4), 2.92(4), 2.985(15)				
Ce–N2/O2 (Å)	2.791(11), 2.910(12), 2.911(12), 2.792(11), 2.396(12), 2.397(12)				
Nb–N1/O1 (Å)	2.0138(5), 2.0138(5)				
Nb–N2/O2 (Å)	2.104(14), 2.072(12), 2.072(12), 2.104(14)				
Bond angles					
∠Nb–N1–Nb (°) (×2)			178.5(17)		
∠Nb–N2–Nb (°) (×4)			150.2(7)		

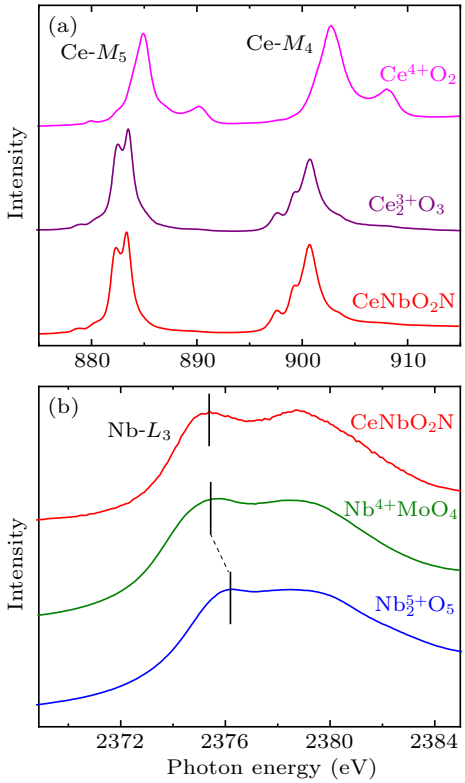

Fig. 2. (a) The Ce-*M* XAS spectra of $CeNbO_2N$ together with a Ce^{4+} reference CeO_2 and a Ce^{3+} reference Ce_2O_3. (b) Nb-L_3 XAS spectra of $CeNbO_2N$ together with a Nb^{4+} reference $NbMoO_4$[32] and a Nb^{5+} reference Nb_2O_5.

The Nb L_3-edge XAS spectrum of $CeNbO_2N$ shifts about 1 eV to the lower energy relative to that of the Nb^{5+} reference Nb_2O_5, but locates at the same energy as that of Nb^{4+} reference compound $NbMoO_4$,[32] demonstrating the Nb^{4+} valence state in $CeNbO_2N$. Therefore, the charge configuration of this sample is determined to be $Ce^{3+}Nb^{4+}O_2N$.

Now, the focus turns to magnetic properties. Figure 3(a) presents the temperature dependence of magnetic susceptibility measured at ZFC and FC modes under a magnetic field of 0.1 T. One finds that these two curves are nearly overlapped with each other. Moreover, no signal of any long-range spin order is observed in the whole temperature range we measured (2–300 K). Above 100 K, the temperature-dependent inverse susceptibility can be fitted based on the Curie–Weiss law with the formula of $(\chi - \chi_0)^{-1} = (T - \theta)/C$, yielding the Weiss temperature $\theta = -33.3$ K and the Curie constant $C = 0.69$ emu·mol^{-1}. Here, χ_0 represents the temperature-independent magnetic susceptibility, such as the Van Vleck paramagnetism and the diamagnetism of the atomic nucleus. According to the fitted Curie constant, the effective magnetic

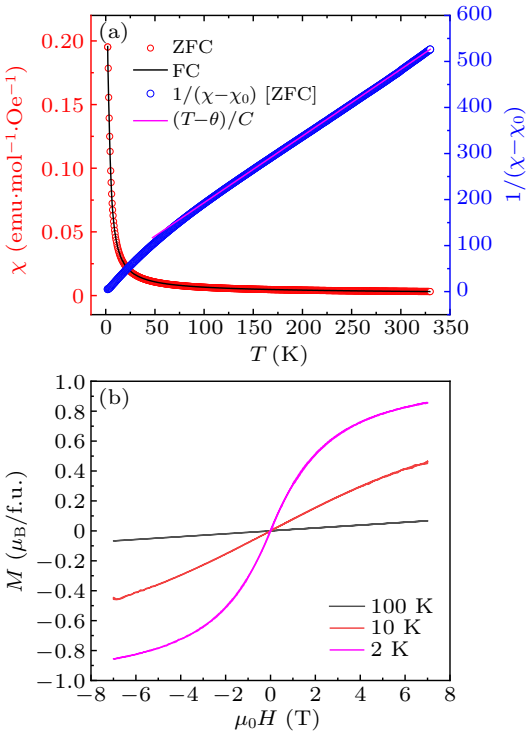

Fig. 3. (a) Temperature dependence of magnetic susceptibility χ measured at 0.1 T with ZFC and FC modes, and the inverse ZFC curve along with the Curie–Weiss fitting above 100 K for $CeNbO_2N$. (b) Field dependent magnetization at fixed temperature.

moment is calculated as $\mu_{\rm eff} = \sqrt{8C} = 2.35\ \mu_{\rm B}$·f.u.$^{-1}$. Note that both Ce^{3+} at the *A*-site and Nb^{4+} at the *B*-site contribute to the magnetic moment, leading to a theoretical effective magnetic moment of $\mu_{\rm th} = \sqrt{g_{J_1}^2 J_1(J_1+1) + g_{J_2}^2 J_2(J_2+1)} = 2.97\ \mu_{\rm B}$·f.u.$^{-1}$ ($J_1 = 5/2$ and $g_{J_1} = 6/7$ for Ce^{3+}; $J_2 = 3/2$ and $g_{J_2} = 4/5$ for Nb^{4+}),[33,34] which is somewhat larger than the experimentally fitted result. This discrepancy suggests the deviation from the totally localized spin moment, indicating the presence of itinerant electronic behavior, due to the $4d^1$ electronic configuration of Nb^{4+}. Figure 3(b) shows the magnetization curves with the magnetic field varying from −7 T to 7 T at some fixed temperature. At 100 K, the linear $M(H)$ feature agrees well with the paramagnetism. At lower temperatures, such as at 2 K, the $M(H)$ curve deviates from the linear behavior,which may suggest the development of some short-range spin correlation or field-induced magnetization.

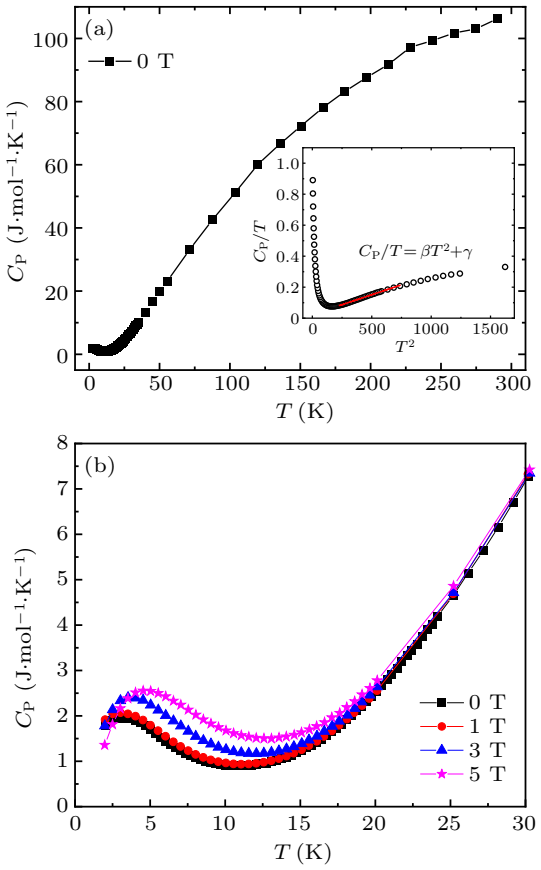

Fig. 4. (a) Temperature-dependent heat capacity of $CeNbO_2N$ measured at zero magnetic field. The inset displays the fitting result (red line) based on the function $C_{\rm P}/T = \beta T^2 + \gamma$ from 15 K to 27 K. (b) Heat capacity measured under various magnetic fields.

Figure 4(a) displays the temperature-dependent specific heat of $CeNbO_2N$ measured in the temperature range of 2–290 K under zero magnetic field. Upon cooling, the specific heat decreases gradually and reaches a minimum around 10 K. With further cooling, the specific heat increases slightly and then decreases again near 4 K, resulting in a dome-like structure. To further explore this specific heat anomaly, a detailed investigation into its magnetic field dependence was conducted. As shown in Fig. 4(b), the specific heat anomaly persists under various magnetic fields and shifts to higher temperatures with increasing fields. This behavior is characteristic of the Schottky anomaly that is usually observed in the rare-earth-based materials.[35–38] Focusing on the low-temperature regime, as depicted by the inset of Fig. 4(a), the specific heat data above the Schottky anomaly temperature (15–27 K) can be fitted with the formula of $C_{\rm P}/T = \beta T^2 + \gamma$, in which the fitted $\beta = 0.26(2)$ mJ·mol·K^{-4}, representing the phonon contributions, and $\gamma = 22.8(9)$ mJ·mol^{-1}·K^{-2}, which is the Sommerfeld coefficient originating from the delocalized electron. The substantial value of the Sommerfeld coefficient γ fitted here indicates a significant electronic contribution to the specific heat, thereby providing additional evidence for the intrinsic metallic nature of $CeNbO_2N$.

To further investigate the behavior of itinerant electrons and their interaction with magnetism, the transport properties of $CeNbO_2N$ were examined using the four-wire method. As illustrated in Fig. 5(a), the compound exhibits lower resistivity values across the measurement temperature range of 2–300 K, although a slight upward trend is found to occur on cooling. Specifically, the resistivity is approximately 7.5 mΩ·cm at 2 K and decreases to 1.9 mΩ·cm at 300 K, indicating the presence of an appreciable amount of itinerant electrons. This observation is in line with the reduced magnetic moment inferred from the susceptibility measurement and the large Sommerfeld coefficient determined by heat capacity analysis. The upturn behavior mentioned above should be attributed to grain boundary effects due to the polycrystalline nature of $CeNbO_2N$, which are usually observed in other polycrystalline samples.[39] This behavior contrasts with that of the intrinsic semiconductor $CeTaN_2O$, the resistivity of which increases dramatically from 2563 Ω·cm at 300 K to 1.4 MΩ·cm at 100 K.[19] Figure 5(b) depicts the magnetoresistance (MR) effect $[MR = 100\% \times (\rho(H) - \rho(0\ {\rm T}))/\rho(0\ {\rm T})]$ of $CeNbO_2N$ as a function of magnetic field at different temperatures. At 10 K, $CeNbO_2N$ exhibits a negligible negative MR effect, suggesting that the magnetic field has minimal impact on carrier scattering caused by disordered spins. However, the MR value reaches 19% at 2 K and 7 T, likely attributed to the development of some short-range spin–spin correlations at higher fields.

The metallicity of $CeNbO_2N$ can be attributed to the presence of Nb^{4+} ions. Nb typically exhibits a +5 valence state with a $4d^0$ electronic configuration. With a fully empty 4d shell, the charge transfer between Nb and other ions is suppressed, resulting in insulating or semiconducting behaviors. For instance, $NaNb^{5+}O_3$, a conventional Nb-based perovskite, shows excellent dielectric properties.[40] The situation is quite different for Nb^{4+} with a $4d^1$ configuration, where the ad-

ditional electron in the 4d orbitals tends to become itinerant when the electronic bandwidth exceeds Coulomb interactions, leading to metallic characteristics. This is indeed the case for $SrNb^{4+}O_3$, which displays well-defined metallic properties.[41,42] In $CeNbO_2N$, the charge mobility is further enhanced by the suppression of Coulomb interactions due to the disordered N/O distributions, resulting in exceptionally low resistivity and a large Sommerfeld coefficient.

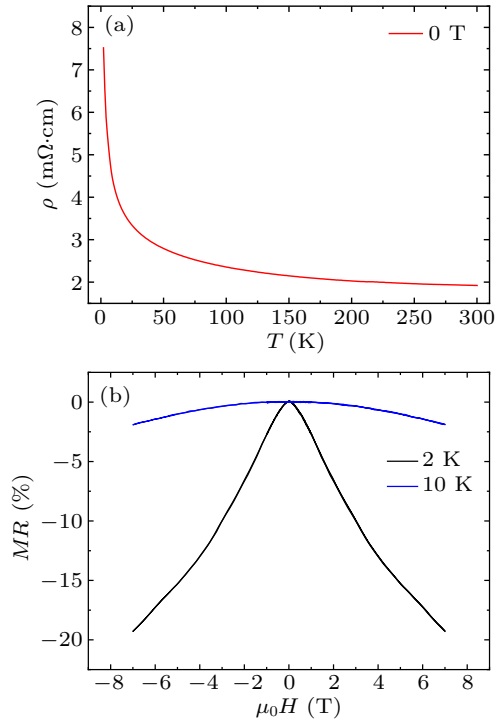

Fig. 5. (a) Zero-field temperature-dependent electrical resistivity of $CeNbO_2N$. (b) Field-dependent magnetoresistance measured at 2 K and 10 K.

4. Conclusions

A new perovskite oxynitride $CeNbO_2N$ was prepared at 3 GPa and 1770 K. Rietveld refinement of SXRD pattern reveals that the compound crystallizes in an orthorhombic structure with the space group *Pnma*. In this structure, the anions exhibit a disordered arrangement, maintaining an elemental ratio of O:N = 2:1. XAS measurements confirm the charge configuration to be $Ce^{3+}Nb^{4+}O_2N$, indicating the presence of a Nb^{4+} charge state with $4d^1$ electronic configuration. No long-range spin order is found to occur by magnetic susceptibility and specific heat measurements, while a Schottky anomaly is observed at lower temperatures. In addition, considerable electronic contribution to low-temperature specific heat is observed in $CeNbO_2N$, suggesting the presence of itinerant electrical behavior as expected from the $4d^1$ electronic configuration of a Nb^{4+} state. In spite of the absence of long-range spin order, remarkable magnetoresistance effect shows up at lower temperature in the current $CeNbO_2N$, which may be ascribed to the development of some short-range spin correlations at moderate magnetic fields.

Acknowledgements

Project supported by the National Key R&D Program of China (Grant No. 2021YFA1400300), the National Natural Science Foundation of China (Grant Nos. 12425403, 12261131499, 12304268, 12304159, 11934017, and 11921004), and the China Postdoctoral Science Foundation (Grant No. 2023M743741). The synchrotron x-ray diffraction experiments were performed at SPring-8 with the approval of the Japan Synchrotron Radiation Research Institute (Grant Nos. 2023B1575, 2023B1976, 2024A1506, and 2024A1695).

References

[1] Hwang J, Rao R R, Giordano L, Katayama Y, Yang Y and Yang S H 2017 *Science* **358** 751
[2] Jia Z Y, Cheng C P, Chen X, Liu L L, Ding R, Ye J L, Wang J, Fu L J, Cheng Y H and Wu Y P 2023 *Mater. Adv.* **4** 79
[3] Xiong C, Li B S, Liao Z X, Qiu Y and Gao D Q 2025 *Chin. Phys. B* **34** 047701
[4] Song W B, Xi G Q, Pan Z, Liu J, Ye X B, Liu Z H, Wang X, Shan P F, Zhang L X, Lu N P, Fan L L, Qin X M and Long Y W 2024 *Chin. Phys. B* **33** 057701
[5] Yen F, Dela Cruz C, Lorenz B, Galstyan E, Sun Y Y, Gospodinov M and Chu C W 2007 *J. Mater. Res.* **22** 2163
[6] Dabrowski B, Kolesnik S, Baszczuk A, Chmaissem O, Maxwell T and Mais J 2005 *J. Solid State Chem.* **178** 629
[7] Qin S J, Zhou B W, Liu Z H, Ye X B, Zhang X Q, Pan Z and Long Y W 2022 *Chin. Phys. B* **31** 097503
[8] Ye X B, Zhao J F, Das H, *et al*. 2021 *Nat. Commun.* **12** 1917
[9] Quan L N, Rand B P, Friend R H, Mhaisalkar S G, Lee T W and Sargent E H 2019 *Chem. Rev.* **119** 7444
[10] Wiesendanger E 1973 *Ferroelectrics* **6** 263
[11] Feng Y J, Chen Y P, Wang L Y, Wang J X, Chang D H, Yuan Y F, Wu M, Fu R J, Zhang L L, Wang Q L, Wang K, Guo H Z and Wang L R 2024 *Chin. Phys. Lett.* **41** 063201
[12] Matsukawa M, Ishikawa R, Hisatomi T, Moriya Y, Shibata N, Kubota J, Ikuhara Y and Domen K 2014 *Nano Lett.* **14** 1038
[13] Yang M H, Oró-Solé J, Kusmartseva A, Fuertes A and Attfield J P 2010 *J. Am. Chem. Soc.* **132** 4822
[14] Tassel C, Kuno Y, Goto Y, Yamamoto T, Brown C M, Hester J, Fujita K, Higashi M, Abe R, Tanaka K, Kobayashi Y and Kageyama H 2015 *Angew. Chem.* **127** 526
[15] Vadapoo R, Ahart M, Somayazulu M, Vadapoo R, Holtgrewe N, Meng Y, Konopkova Z, Hemley R J and Cohen R E 2017 *Phys. Rev. B* **95** 214120
[16] Kim Y I, Woodward P M, Baba-Kishi K Z and Tai C W 2004 *Chem. Mater.* **16** 1267
[17] Jorge A B, Oró-Solé J, Bea A M, Mufti N, Palstra T T M, Rodgers J A, Attfield J P and Fuertes A 2008 *J. Am. Chem. Soc.* **130** 12572
[18] Porter S H, Huang Z G, Cheng Z X, Avdeev M, Chen Z X, Dou S X and Woodward P M 2015 *J. Solid State Chem.* **226** 279
[19] Chen Z L, Lu D B, Ye X B, Zhao H T, Zhang J, Pan Z, Chi Z H, Cui T, Shen Y and Long Y W 2024 *Acta Phys. Sin.* **73** 080702 (in Chinese)
[20] Kloß S D, Weidemann M L and Attfield J P 2021 *Angew. Chem. Int. Ed.* **60** 22260
[21] Talley K R, Perkins C L, Diercks D R, Brennecka G L and Zakutayev A 2021 *Science* **374** 1488
[22] Kim Y I and Lee E 2011 *J. Ceram. Soc. Jpn.* **119** 371
[23] Kim Y I, Si W, Woodward P M, Sutter E, Park S and Vogt T 2007 *Chem. Mater.* **19** 618
[24] Zhang Y R, Motohashi T, Masubuchi Y and Kikkawa S 2011 *J. Ceram. Soc. Jpn.* **119** 581
[25] Santoro A, Marezio M, Roth R S and Minor D 1980 *J. Solid State Chem.* **35** 167
[26] Von Dreele R B 1997 *J. Appl. Crystallogr.* **30** 517
[27] Mitra C, Hu Z, Raychaudhuri P, Wirth S, Csiszar S I, Hsieh H H, Lin H J, Chen C T and Tjeng L H 2003 *Phys. Rev. B* **67** 092404

[28] Howald L, Stilp E, De Réotier P D, Yaouanc A, Raymond S, Piamonteze C, Lapertot G, Baines C and Keller H 2015 *Sci. Rep.* **5** 12528
[29] Strigari F, Willers T, Muro Y, Yutani K, Takabatake T, Hu Z, Agrestini S, Kuo C Y, Chin Y Y, Lin H J, Pi T W, Chen C T, Weschke E, Schierle E, Tanaka A, Haverkort M W, Tjeng L H and Severing A 2013 *Phys. Rev. B* **87** 125119
[30] Chen J M, Chin Y Y, Valldor M, Hu Z, Lee J M, Haw S C, Hiraoka N, Ishii H, Pao C W, Tsuei K D, Lee J F, Lin H J, Jang L Y, Tanaka A, Chen C T and Tjeng L H 2014 *J. Am. Chem. Soc.* **136** 1514
[31] Burnus T, Hu Z, Wu H, Cezar J C, Niitaka S, Takagi H, Chang C F, Brookes N B, Lin H J, Jang L Y, Tanaka A, Liang K S, Chen C T and Tjeng L H 2008 *Phys. Rev. B* **77** 205111
[32] Ji Y, Wang W F, Ding Y F, Wang H X, Yang J K, Guo Q W, Ye X B, Shen X, Yao Y, Zhao J F, Jin C Q, Chan T S, Hu Z W, Long Y W and Yu R C 2022 *J. Phys.: Condens. Matter* **628** 413624
[33] Mugiraneza S and Hallas A M 2022 *Commun. Phys.* **5** 95
[34] Martins C, Aichhorn M and Biermann S 2017 *J. Phys.: Condens. Matter* **29** 263001
[35] Pathak A K, Paudyal D, Mudryk Y, Gschneidner K A and Pecharsky V K 2013 *Phys. Rev. Lett.* **110** 186405
[36] Ranaut D and Mukherjee K 2022 *J. Phys.: Condens. Matter* **34** 315802
[37] Shao M J, Cao S X, Wang Y B, Yuan S J, Kang B J, Zhang J C, Wu A H and Xu J 2011 *J. Cryst. Growth* **318** 947
[38] Cheng J G, Sui Y, Qian Z N, Liu Z G, Miao J P, Huang X Q, Lu Z, Li Y, Wang X J and Su W H 2005 *Solid State Commun.* **134** 381
[39] Kobayashi K I, Kimura T, Sawada H, Terakura K and Tokura Y 1998 *Nature* **395** 677
[40] Shanker V, Samal S L, Pradhan G K, Narayana C and Ganguli A K 2009 *Solid State Sci.* **11** 562
[41] Oka D, Hirose Y, Nakao S, Fukumura T and Hasegawa T 2015 *Phys. Rev. B* **92** 205102
[42] Wei H R, Chen S R, Zou Y T, Wang Y X, Yang M, Zhang Q H, Zou K, Gu L, Jiang K, Guo E J and Cheng Z G 2024 *Phys. Rev. B* **109** 205404